Transition from ultrafast laser photo-electron emission to space-charge-limited current in a 1D gap

2014 J. Phys. D: Appl. Phys. 47 125502

(http://iopscience.iop.org/0022-3727/47/12/125502)

J. Phys. D: Appl. Phys. 47 (2014) 125502 (7pp) doi:10.1088/0022-3727/47/12/125502

Transition from ultrafast laser photo-electron emission to space-charge-limited current in a 1D gap

Yangjie Liu[1] **and L K Ang**[2]

[1] School of Electrical and Electronic Engineering, Nanyang Technological University, Singapore 639798, Singapore
[2] Engineering Product Development, Singapore University of Technology and Design, Singapore 138682, Singapore

E-mail: ricky_ang@sutd.edu.sg

Received 11 October 2013, revised 16 January 2014
Accepted for publication 27 January 2014
Published 6 March 2014

Abstract

A one-dimensional (1D) model has been constructed to study the transition of the time-dependent ultrafast laser photo-electron emission from a flat metallic surface to the space-charge-limited (SCL) current, including the effect of non-equilibrium laser heating on metals at the ultrafast time scale. At high laser field, it is found that the space charge (SC) effect cannot be ignored and the SCL current emission is reached at a lower value predicted by a short-pulse SCL current model that has assumed a time-independent emission process. The threshold of the laser field to reach the SCL regime is determined over a wide range of operating parameters. The calculated results agree well with particle-in-cell simulation results. It is found that the SC effect is more important for materials with lower work function like tungsten (4.4 eV) as compared with gold (5.4 eV). However, for a flat surface, both materials will reach the SC limited regime at sufficient high laser field such as >5 GV m^{-1} with a laser pulse length of 10 s to 100 fs.

Keywords: electron emission, multiphoton absorption, space-charge-limited current, ultrafast laser excited electron

(Some figures may appear in colour only in the online journal)

1. Introduction

For electrons emitted from a surface into a free space, the amount of current emitted at low-current regime is dominated by the emission mechanism, which is known as source-limited emission. The mechanism can be divided into three types, namely thermionic emission, field emission and photoemission, which are, respectively, described by the Richardson–Laue–Dushman (RLD) law [1], the Fowler–Nordheim (FN) law [2], and the Fowler–Dubridge (FD) law [3–5]. A good overview can be found in a recent paper by Jensen [6]. In particular, all three emission mechanisms can be combined in a generalized model [7].

At high-current regime, the amount of the emitted current will be influenced by the space charge (SC) effect, and it is known as the space-charge-limited (SCL) current, which describes the maximum current density allowed for steady-state electrons emitted from the cathode and transported across the gap. For a one-dimensional (1D) gap of spacing D and a dc voltage of V_g, the SCL current is governed by the 1D classical Child–Langmuir (CL) law [8, 9], given by

$$J_{CL} = \frac{4\epsilon_0}{9D^2}\sqrt{\frac{2e}{m}}V_g^{3/2}, \tag{1}$$

where ϵ_0, e and m are, respectively, vacuum permittivity, electron charge and electron mass. SCL electron flow occurs when the charge of the emitted electrons is sufficient to suppress the electric field at the cathode to zero, and the electrostatic potential distribution function $\phi(x)$ is

$$\phi(x) = V_g\left(\frac{x}{D}\right)^{4/3}. \tag{2}$$

The transition from source-limited emission to SCL current is important in the development of cathodes such as field emitters and photocathode, which are, respectively, based on field emission and photoemission. The transition from the field emission to SCL current has been developed for large [10] and small [11] gaps. For the transition from photoemission to SCL current, the CL law cannot be used directly, because the pulse length of the electron photoemission is normally much smaller than the electron transit time across the gap. This short-pulse effect on the CL law has been developed in a 1D classical model [12] given by

$$J_{\mathrm{crit}} = 2\frac{1-\sqrt{1-\frac{3}{4}X_{\mathrm{CL}}^2}}{X_{\mathrm{CL}}^3}J_{\mathrm{CL}}, \tag{3}$$

where $X_{\mathrm{CL}} = \tau_{\mathrm{p}}/\tau$ (<1) is the normalized pulse length and $\tau = 3D\sqrt{m/2eV_{\mathrm{g}}}$ is the transit time under the SCL condition. A more recent model has also been developed to include the quantum effects when the electron de Broglie wavelength is comparable or smaller than the electron pulse width [13].

Recently, significant efforts have been made in using ultrafast lasers to induce electron photo-field emission from metallic tips [14–29]. In most studies, the SC effect has been ignored, which may be important at high-current regime operating at high laser fields [30, 31]. Depending on the operating conditions, the emission process due to ultrafast laser excitation can be complicated, which leads to multiphoton emission [16], optical tunnelling [14], strong-field photoemission [21], and above-threshold photoemission [19]. The onset of the optical tunnelling from the multiphoton emission can be determined by a formula [22], which is at about 9.81 V nm^{-1} for an 8 fs laser pulse.

In this paper, we only focus on the photoemission process, and we are interested in developing a simple and 1D model to show the transition from the ultrafast-laser-induced multiphoton emission to the SCL at ultrafast time scale. Due to the long relaxation time scale (ps), the multiphoton emission process is governed by the non-equilibrium heating model [18], which has shown that the emission is time dependent at a time scale less than 1 ps for metals. Note that this phenomenon has been verified by an experiment in 2011 [20].

While equation (3) is able to account for the effect of a short pulse, yet it has assumed that the current injected into the gap is time independent. Here, from $t = 0$ (beginning of the laser pulse) to $t = \tau_{\mathrm{p}}$ (end of the pulse), the injected current density from the cathode at $x = 0$ is emitted as a function of time, given by $J(t)$. To solve this problem, we need to find the spatial variation of the injected electron density into the gap, $J(x)$ for $0 \leqslant x \leqslant s$, where s $(\ll D)$ is the position of the beam front at $t = \tau_{\mathrm{p}}$. Once this $J(x)$ is obtained, we may use the similar approach in the short-pulse model [12] to calculate the SCL electron flow for the ultrafast-laser-induced photo-field emission.

It is important to note that the model presented here has ignored the sharpness of the tip, thus the prediction can be considered only as a zero-order estimation. While the 2D CL law has been developed [32], it cannot be applied directly as the emitting area (in a sharp tip) is much smaller than the gap spacing. The model is a quantitative one that is able to compare experiments using ultrafast lasers to excite multiphoton electron emission from a flat surface. In future, it can be extended to a non-uniform and at least a 2D model to account for the sharpness of the tip in order to compare quantitatively with the experiments using sharp tips. Note that the latter is not a trivial task, as there is no protrusive CL law which is valid for even steady-state electron emission from a sharp tip.

2. Model

Consider a gap of spacing D with an external fixed electric field $F_{\mathrm{dc}} = V_{\mathrm{g}}/D$. The cathode (at $x = 0$) is excited by an ultrafast laser to induce electron emission with a time-varying current density $J(t)$. The emitted electrons will travel under the influence of the electric field (including SC field) to reach a distance of s $(< D)$ within the laser pulse length τ_{p}, which is smaller than the transit time τ. Note that the laser profile is a step-like function with a laser duration of τ_{p}.

In the region of $0 \leqslant x \leqslant s$, the electrostatic potential is

$$\phi(0 \leqslant x \leqslant s) = F_{\mathrm{dc}}x + \Delta\phi(x), \tag{4}$$

where $\Delta\phi(x)$ is the space-charge electrostatic potential. The value of s can be calculated by solving the equation of motion for $x(t)$ given by

$$\frac{\mathrm{d}^2}{\mathrm{d}t^2}x(t) = \frac{e}{m}\left[F_{\mathrm{dc}} + \frac{\mathrm{d}}{\mathrm{d}x}\Delta\phi(x)\right], \tag{5}$$

with initial conditions: $x(t = 0) = 0$ and $x'(t = 0) = v_0 \approx 0$. Here, the initial velocity v_0 is kept to be reasonably small (but not equal to 0) to avoid the difficulty in the numerical integration of the Poisson equation (see below) at $x = 0$. In general, we have $v_0\tau_{\mathrm{p}} \ll s$ in our calculation.

Near the cathode surface, we consider that there is a surface potential barrier,

$$V(x) = V_{\mathrm{f}} + \Phi - \frac{e^2}{16\pi\epsilon_0 x} - exF_{\mathrm{dc}} - e\Delta\phi(x). \tag{6}$$

where V_{f} is the Fermi energy, Φ is its work function and the third term is the classical image charge potential. Using equation (6), we obtain that the time-dependent tunnelling current density $J(t)$, which is calculated from using

$$J(t) = \frac{em}{2\pi^2\hbar^3}\int_0^{\infty}\mathrm{d}W\,T(W)\int_W^{\infty} f(E,t)\,\mathrm{d}E. \tag{7}$$

Here, $T(W)$ is the electron tunnelling probability at energy level (W) through the surface potential barrier (see equation (6)), which is based on the modified Wentzel–Kramers–Brillouin (WKB) method, $f(E,t)$ is the time-varying non-equilibrium electron distribution function based on our previous model [18], W is a dummy variable in the integration, and $\hbar$ is the reduced Plank constant. The details on how to obtain $T(W)$ and $f(E,t)$ can be found in [18, 22].

Using equation (7), the emitted charge density (per unit area) within the laser pulse width is calculated by

$$\sigma_{\mathrm{EC}} = \int_0^{\tau_{\mathrm{p}}} J(t)\,\mathrm{d}t. \tag{8}$$

To determine $\Delta\phi(x)$ in the region of $0 \leqslant x \leqslant s$, we solve the Poisson equation,

$$\frac{\mathrm{d}^2}{\mathrm{d}x^2}\Delta\phi(x) = \frac{J(x)}{\epsilon_0 v(x)}, \tag{9}$$

where $v(x)$ is the velocity profile of the electron flow that can be obtained using the energy conservation,

$$\frac{mv^2(x)}{2} = e[F_{\mathrm{dc}}x + \Delta\phi(x)]. \tag{10}$$

Here, $J(x)$ is the current density profile obtained at the end of the pulse at $t = \tau_{\mathrm{p}}$, which is related to equation (7), and it can be expressed as

$$J(x) = J[\tau_{\mathrm{p}} - t(x)], \tag{11}$$

where $t(x)$ is the inverse function of $x(t)$ solved in equation (5). Combining equations (9) to (11), we have

$$\frac{\mathrm{d}^2}{\mathrm{d}x^2}\Delta\phi(x) = \frac{J[\tau_{\mathrm{p}} - t(x)]}{\sqrt{\frac{2e}{m}(F_{\mathrm{dc}}x + \Delta\phi(x))}}. \tag{12}$$

The boundary conditions for solving equation (12) are the zero space potential at the cathode ($x = 0$) and the continuous electric field at the beam front ($x = s$), which are respectively,

$$\Delta\phi(0) = 0, \tag{13}$$

and

$$\frac{\mathrm{d}}{\mathrm{d}x}\Delta\phi(x)|_{x=s} = -\frac{\Delta\phi(s)}{D-s}. \tag{14}$$

Note that equation (14) is reduced from $\mathrm{d}\phi(\mathrm{x})/\mathrm{d}x|_{x=s} = (V_{\mathrm{g}} - \phi(s))/(D-s)$. Finally, the electrostatic potential in the vacuum region of $s < x \leqslant D$ (in front of the electron beam) is

$$\Delta\phi(s \leqslant x \leqslant D) = \frac{\Delta\phi(x=s)}{D-s}(D-x). \tag{15}$$

From the equations, it is required to solve $\Delta\phi(x)$, s and $x(t)$ numerically to determine the SCL current density $J(t)$ or the SCL charge density σ_{EC} consistently. Here we construct a *numerical* algorithm to perform the calculation iteratively.

On the first step, we assume $\Delta\phi_1(x) = 0$ in equation (6) to obtain the electron current density (without SC effects) $J_1(t)$ from equation (7), which gives the first estimated value for $J(t)$. By substituting $\Delta\phi = 0$ into equation (5), we also obtain the first estimated time-profile $x(t)$ and hence its inverse function $t(x)$. Here the value of s is determined by $s = x$ $(t = \tau_{\mathrm{p}})$. With this $J_1(t)$, we can solve the Poisson equation from equation (12) for the new $\Delta\phi_2(x)$, which can be used to estimate the new current density $J_2(t)$. Here, $J_2(t)$ is different from $J_1(t)$ due to the finite value of $\Delta\phi_2(x)$ as the SC effect has been included. The iterative process will continue until a convergence is reached which is determined by $|J_{i+1}(t=\tau_{\mathrm{p}}) - J_i(t=\tau_{\mathrm{p}})|/J_i(t=\tau_{\mathrm{p}}) \leqslant 1.5\times10^{-4}$, where i is the iterative step. Once the convergence is reached, we can determine the SC field $\Delta\phi(x)$, and compute the SCL charge density σ_{EC} according to equation (8), which can be compared with our previous work that had excluded the SC effects completely [18].

It is important to note that this approach has ignored completely the SC field within the short time scale less than τ_{p}. The approach is similar to the short-pulse model with constant current density J [12], which had been confirmed with particle-in-cell (PIC) code. Our results will also be compared with PIC simulation with a time-dependent emission current, which shows rather good agreement.

Before presenting the results, we are interested to calculate the saturation of the SCL current density at high fields due to the suppression of the *total* electric field towards zero at the cathode. Thus the SC potential $\Delta\phi(x)$ must be large enough to suppress the applied dc field F_{dc}, which is given by

$$F_{\mathrm{dc}} = -\frac{\mathrm{d}}{\mathrm{d}x}\Delta\phi|x=0. \tag{16}$$

When the above condition is fulfilled, we define a critical (or SCL) current density,

$$J_{\mathrm{SCL}}(t) = fJ_0(t), \tag{17}$$

where f is an enhancement factor over the current density J_0 obtained from the time-dependent ultrafast laser emission model (without SC effects) [18]. Here, f can be expressed by

$$f = -\frac{F_{\mathrm{dc}}}{\frac{\mathrm{d}}{\mathrm{d}x}\Delta\phi_0(x=0)}, \tag{18}$$

where $\Delta\phi_0$ is the SC potential obtained by solving the Poisson equation using $J_0(t)$.

3. Results and discussions

We will not present the calculated $f(E,t)$ in this paper. It is due to a step-function like ultrafast profile, and has been shown elsewhere (see figure 1 in [18]). The property of the $f(E,t)$ for a Gaussian-like ultrafast laser profile can also be found in a recent publication (see figure 1 in [22]). From these calculated $f(E,t)$, we solve equations (6), (7) and (12) to obtain a self-consistent J including the SC effect, which is linked to the emission process and also the non-equilibrium laser–metal interaction at ultrafast time scale. A more recent model on the non-equilibrium laser-metal interaction can also be found in [28].

In figure 1, we present the emitting charge density σ_{EC} as a function of laser field F_{L} with the following parameters: $\tau_{\mathrm{p}} = 50$ fs, $F_{\mathrm{dc}} = 1\,\mathrm{GV\,m^{-1}}$, $D = 1\,\mu$m and $\Phi = 4.4$ eV. In the figure, we see that at the low laser field $F_{\mathrm{L}} < 5\,\mathrm{GV\,m^{-1}}$, both σ_{EC} values calculated by models with (red squares) and without SC effect (black circles) are nearly identical, which indicates SC effects are not important in this range of low F_{L}. Around $F_{\mathrm{L}} = 5\,\mathrm{GV\,m^{-1}}$, we see a smooth transition into the

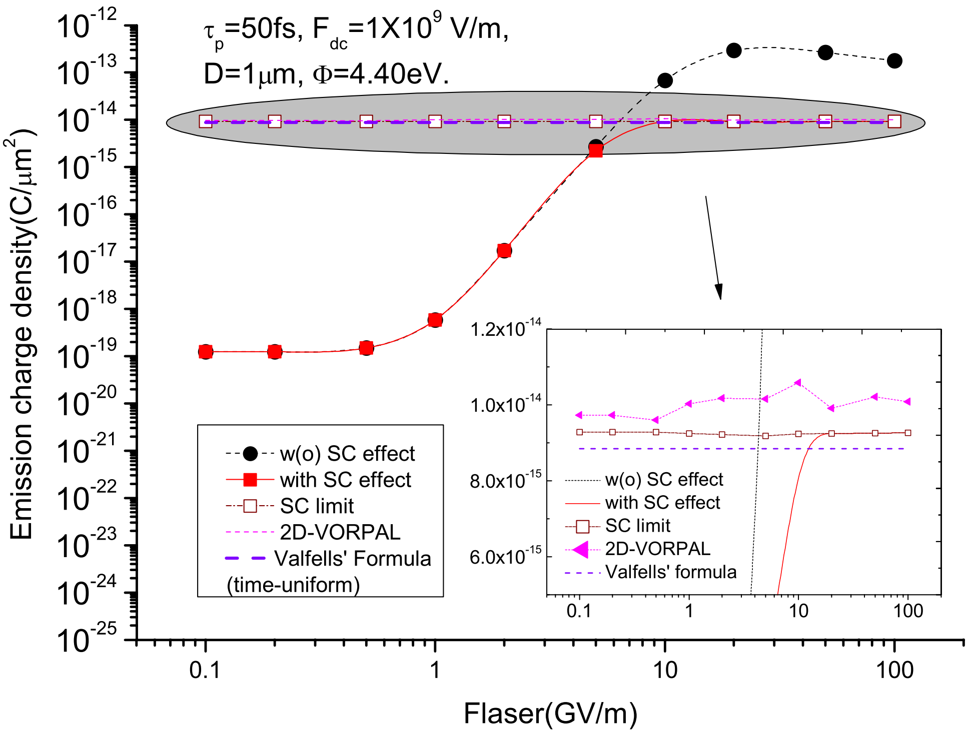

Figure 1. Emission charge density σ_{EC} as a function of laser field F_L for cases with (red solid square) and without the SC effect (black dot) at $\tau_p = 50$ fs, $F_{dc} = 1\,\text{GV m}^{-1}$, $D = 1\,\mu$m, $\Phi = 4.4$ eV. The comparisons are the SC limit from (17), Valfells' formula [12] and 2D VORPAL (PIC simulation results). Inset: enlargement of the shaded region near the SCL regime.

SCL regime (SC limits indicated in open square) (also see the inset of figure 1 which zooms in the shaded oval zone). In comparison with the time-independent model (dashed purple line) by Valfells *et al* [12], our results (time-dependent) of SC limit are slightly higher.

Above the threshold laser field, increasing laser power will not further increase the emitted charge, and the limit is determined by the SCL current. In this regime, the amount of charge density remains as a constant, which is simply controlled by $Q = C \times V_g$, where C is is the capacitance per area of the gap.

To compare our results with PIC simulation, we use a 2D PIC code called VORPAL [33]. In the simulation, we inject a time-dependent electron current density based on our model [18], and we determine the SCL current when reflection of electrons is detected [34, 35]. In the simulation, we have a large emitting area so that the electron flow has a uniform space distribution in the transverse directions in order to compare with our 1D model. The comparison shows that our model (open square) is slightly lower than the PIC simulation results (triangle) as shown in the inset of figure 1. Because both our method and PIC simulation give higher emission densities than Valfells' formula does, this demonstrates or at least inspires one to ponder whether it is possible to achieve a higher upper limit of SCL emission density in the time-dependent injection current case.

In figure 2, we plot the SC potential $\Delta\phi(x)$ in the region electrons distribute $0 < x/s < 1$ for $F_L = 2\,\text{GV m}^{-1}$ (figure 2(*a*)) and $=5\,\text{GV m}^{-1}$ (figure 2(*b*)) based on the same parameters used in figure 1. It is clear that the SC effect can be ignored for $F_L = 2\,\text{GV m}^{-1}$, where the magnitude of $\Delta\phi(x)$ is much less than than the one based on $F_L = 5\,\text{GV m}^{-1}$ by two orders of magnitude. The corresponding emitting current density is plotted in figures 2(*c*) and (*d*), respectively. This figure confirms our observation above that the critical point for the SC effect to dominate is around $\sim 5\,\text{GV m}^{-1}$ under the physical situation investigated in figure 1.

In figure 3, we study the dependence of our results by varying the work function Φ, dc field F_{dc} and laser pulse length τ_p. Here, the gap spacing is fixed at $D = 1$ cm. In figures 3(*a*)–(*c*), we present the cases at $\tau = 10$ fs for $F_{dc} = 1\,\text{MV m}^{-1}$, $1\,\text{GV m}^{-1}$ and $3\,\text{GV m}^{-1}$ (left to right). On each panel of figure 3, we show three calculations at different work functions $\Phi = 2.2$, 4.4 and 5.4 eV. Figures 3(*d*)–(*f*) are presented similarly to figures 3(*a*)–(*c*), except at longer laser pulse $\tau_p = 100$ fs. By comparing the six panels of figure 3, we make the following observations and discussions.

From the results, we can see that a higher work function (like 5.4 eV) will enter the SCL regime at a higher laser field. However, the difference between 5.4 and 4.4 eV is not significant. Both cases will be in the SCL regime at $F_L > 5\,\text{GV nm}^{-1}$. Thus, we expect that experiments using gold with a higher work function (5.4 eV) than tungsten (4.4 eV) will have fewer SC effects at a fixed laser field.

As the laser field increases from $F_L = 0.1$ to $100\,\text{GV m}^{-1}$, the emission charge density σ_{EC} increases within the small F_L range and it gradually saturates to the SCL regime at the high F_L range as expected. The critical value of F_L that SC effects become important (thus also the threshold to reach SC limit) is dependent on all three parameters F_{dc}, Φ and τ. In general, it is easy to reach the SCL regime (critical value of F_L is small) for small Φ, and low F_{dc}. At small Φ, it is easy

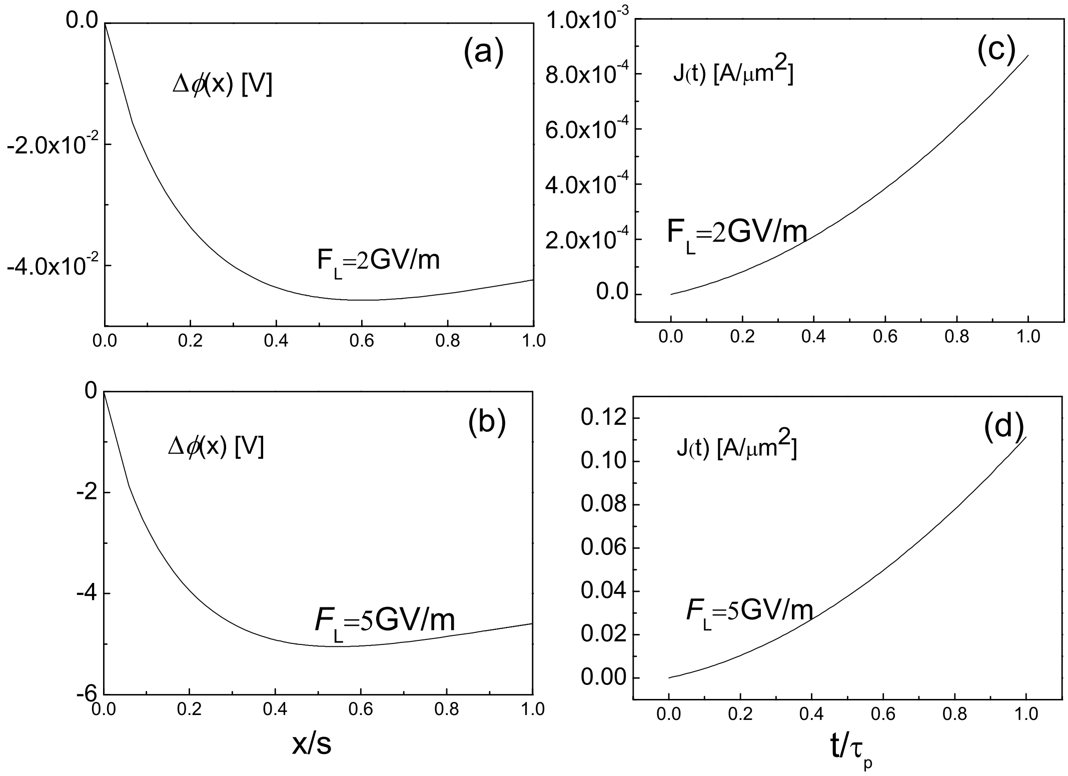

Figure 2. The SC potential profile ($\Delta\phi(0 \leqslant x/s \leqslant 1)$) at two different laser fields $F_L = 2\,\mathrm{GV\,m^{-1}}$ (*a*) and $5\,\mathrm{GV\,m^{-1}}$ (*b*). The corresponding time-dependent emitting current density $J(t)$ is plotted in (*c*) and (*d*). The parameters used are same as those in figure 1.

to have a large emission current at a fixed field, so an SC limit may also be reached at low F_L values, naturally consistent with our expectation because a lower work function makes the tunnelling of electrons easier. For example, the critical value to reach the the SCL regime (show in figure 3(*a*)) is about F_L 1 to $2\,\mathrm{GV\,m^{-1}}$ for $\Phi = 2.2\,\mathrm{eV}$ as compared with $F_L = 5$ to $10\,\mathrm{GV\,m^{-1}}$ for $\Phi = 4.4$ to $5.4\,\mathrm{eV}$.

At small F_{dc} and fixed D, SCL current is small, so it is easy to reach the SCL regime for a given emission current. As F_{dc} increases, emission is significantly promoted because tunnelling probability increases as shown in equation (6). However, the SCL current density also increases with F_{dc}. For example, the critical value to reach the SCL regime ($\Phi = 2.2\,\mathrm{eV}$ case) is about $F_L = 1\,\mathrm{GV\,m^{-1}}$ (at $F_{dc} = 1\,\mathrm{MV\,m^{-1}}$ in figure 3(*a*)) as compared with $F_L = 2\,\mathrm{GV\,m^{-1}}$ (at $F_{dc} = 3\,\mathrm{GV\,m^{-1}}$ in figure 3(*c*)). Thus the dependence on the dc field is not as sensitive as compared with work function Φ.

The total amount of the SCL charge density σ_{EC} (within the laser pulse) is found to be nearly identical for various $\tau_p = 10$ to 100 fs (see the blue dashed lines labelled SC limit). While the SCL charge current density is expected to increase with small τ_p according to both a short pulse [12] and the models here, the total amount of SCL emitted charge integrated over the small laser pulse length will cancel the short-pulse enhancement of current density. This is understandable as the total amount of charge emitted under SCL will depend on the surface electric field on the cathode [36]. The critical value for the laser field to reach the SC limit will be lower at a longer pulse duration of the electron flow.

Finally, it is important to note that the SCL current density calculated here is based on a 1D model that does not account for the sharpness of the tip as mentioned in the Introduction. It is expected that the value will be enhanced by a factor of 20 to 100 for a very sharp tip (see figure 8 in [37]). Based on this, if we assume that the SCL current density is enhanced by a factor of 50, then the threshold of the laser field to reach the SCL current may be increased from $5\,\mathrm{GV\,m^{-1}}$ (for a flat surface in figure 1) to about $10\,\mathrm{GV\,m^{-1}}$ (for a sharp tip) in order to reach the higher SCL current density. Note that this estimation is only a zero-order approximation; accurate results will require a protrusive SCL current model, which is beyond the scope of this paper.

4. Summary

In summary, we have developed a 1D model to study the space-charge-limited (SCL) emission under the ultrafast laser-induced-electron emission due to multiphoton absorption and non-equilibrium laser heating on a flat metal surface. Our model indicates that space-charge effects may *not* be ignored for the high laser field and the threshold to reach the SCL regime is determined for various parameters such as work function, dc applied field and laser pulse length. Smooth transition from the source-limited emission to SCL current is obtained. The calculated results are compared with PIC simulation and a short-pulse SCL current model [12]. It is found that the space-charge effect is more important for materials with lower work function like tungsten (4.4 eV) as compared with gold (5.4 eV). However, for a flat surface, both materials will reach the SCL regime at sufficient high laser

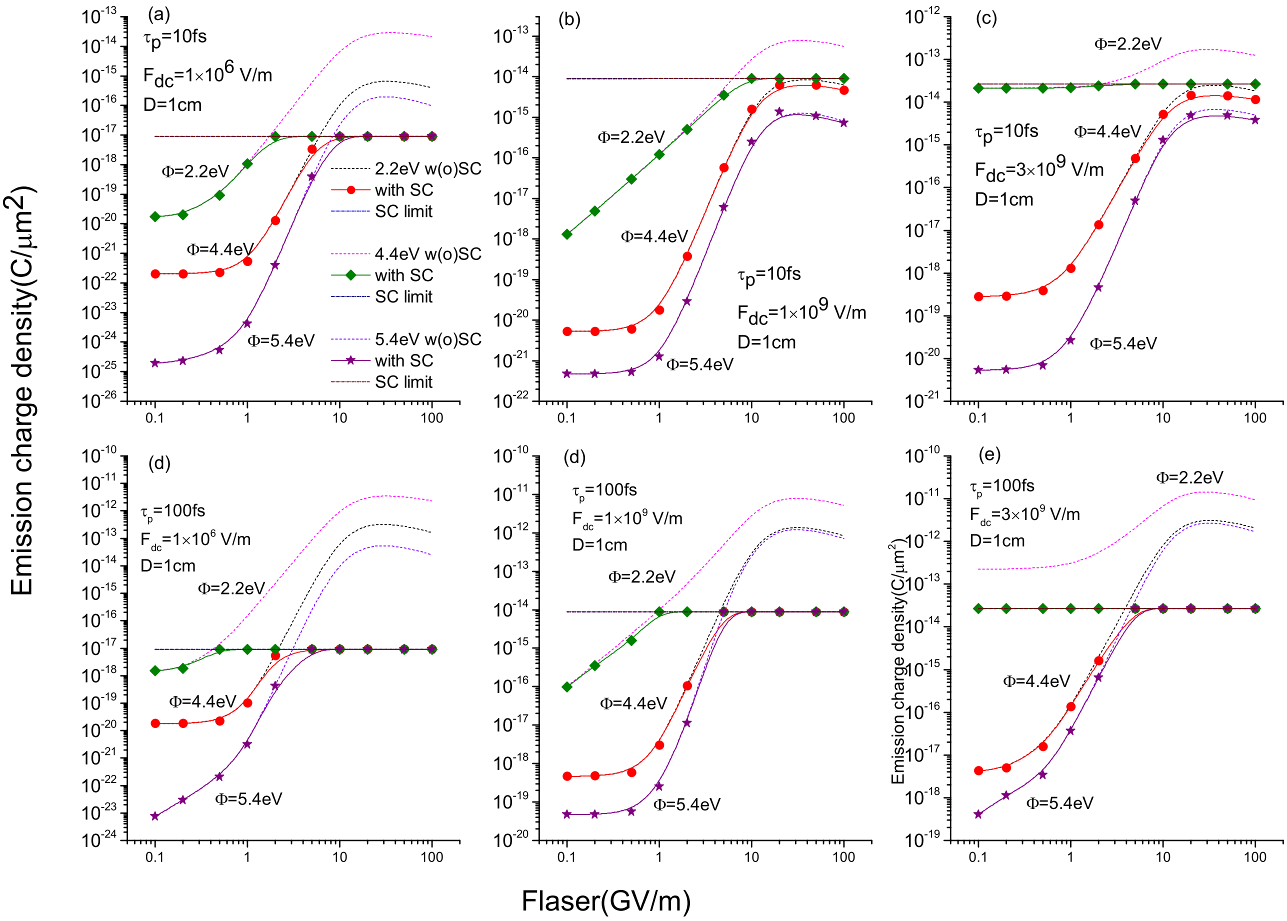

Figure 3. (*a*)–(*f*) Emission charge densities σ_{EC} as a function of laser field $F_L = 0.1$ to 100 GV m^{-1} at $\tau = 10$ fs (top) and 100 fs (bottom) for for different dc fields $F_{dc} = 1$ MV m^{-1}, 1 GV m^{-1} and 3 GV m^{-1} (left to right). In each figure, the calculations are performed for $\Phi = 2.2$ eV (green symbols), 4.4 eV (red symbols) and 5.4 eV (purple symbols). (The gap spacing is fixed at $D = 1$ cm at all cases and the legend in (*a*) applies to (*b*)–(*f*) also.)

field such as >5 GV m^{-1} with a laser pulse length of 10 s to 100 fs.

Acknowledgments

This work was supported by computing server of Institute of High Performance Computing, Agency for Science, Technology and Research (IHPC, A*STAR), Singapore. This project is funded by the Singapore MOE Tier 2 grant (MOE2008-T2-01-033) and USA AFOAR AOARD grant (11-4069). LY thanks Liang Shijun for his assistance to perform this calculation work.

References

[1] Richardson O W 1921 *The Emission of Electricity from Hot Bodies* (New York: Longmans, Green)
[2] Fowler R H and Nordheim L 1928 Electron emission in intense electric fields *Proc. R. Soc. London* A **119** 173
[3] Fowler R H 1931 The analysis of photoelectric sensitivity curves for clean metals at various temperatures *Phys. Rev.* **38** 45
[4] DuBridge L A 1932 A further experimental test of Fowler's theory of photoelectric emission *Phys. Rev.* **39** 108
[5] DuBridge L A 1933 Theory of the energy distribution of photoelectrons *Phys. Rev.* **43** 727
[6] Jensen K L 2007 *Advances in Imaging and Electron Physics* (Singapore: Elsevier)
[7] Jensen K L, O'Shea P G and Feldman D W 2002 Generalized electron emission model for field, thermal and photoemission *Appl. Phys. Lett.* **81** 3867
[8] Child C D 1911 Discharge from hot CaO *Phys. Rev. (Series 1)* **32** 492–511
[9] Langmuir I 1913 The effect of space charge and residual gases on thermionic currents in high vacuum *Phys. Rev.* **2** 450–86
[10] Lau Y Y, Liu Y and Parker R K 1994 Electron emission: from the Fowler–Nordheim relation to the Child–Langmuir law *Phys. Plasmas* **1** 2082
[11] Koh W S and Ang L K 2006 Transition of field emission to space-charge-limited emission in a nano gap *Appl. Phys. Lett.* **89** 183107
[12] Valfells Á, Feldman D W, Virgo M, O'Shea P G and Lau Y Y 2002 Effects of pulse-length and emitter area on virtual cathode formation in electron guns *Phys. Plasmas* **9** 2377–82
[13] Ang L K and Zhang P 2007 Ultrashort-pulse Child–Langmuir law in the quantum and relativistic regimes *Phys. Rev. Lett.* **98** 164802
[14] Hommelhoff P, Sortais Y, Aghajani-Talesh A and Kasevich M A 2006 Field emission tip as a nanometer source of free electron femtosecond pulses *Phys. Rev. Lett.* **96** 4

[15] Hommelhoff P, Kealhofer C and Kasevich M A 2006 Ultrafast electron pulses from a tungsten tip triggered by low-power femtosecond laser pulses *Phys. Rev. Lett.* **97** 4
[16] Ropers C, Solli D R, Schulz C P, Lienau C and Elsaesser T 2007 Localized multiphoton emission of femtosecond electron pulses from metal nanotips *Phys. Rev. Lett.* **98** 043907
[17] Barwick B, Corder C, Strohaber J, Chandler-Smith N, Uiterwaal C and Batelaan H 2007 Laser-induced ultrafast electron emission from a field emission tip *New J. Phys.* **9** 142
[18] Wu L and Ang L K 2008 Nonequilibrium model of ultrafast laser-induced electron photofield emission from a dc-biased metallic surface *Phys. Rev.* B **78** 224112
[19] Schenk M, Krüger M and Hommelhoff P 2010 Strong-field above-threshold photoemission from sharp metal tips *Phys. Rev. Lett.* **105** 257601
[20] Yanagisawa H, Hengsberger M, Leuenberger D, Klöckner M, Hafner C, Greber T and Osterwalder J 2011 Energy distribution curves of ultrafast laser-induced field emission and their implications for electron dynamics *Phys. Rev. Lett.* **107** 087601
[21] Yalunin S, Gulde M and Ropers C 2011 Strong-field photoemission from surfaces: theoretical approaches *Phys. Rev.* B **84** 195426
[22] Pant M and Ang L K 2012 Ultrafast laser-induced electron emission from multiphoton to optical tunneling *Phys. Rev.* B **86** 045423
[23] Ang L K and Pant M 2013 Generalized model for ultrafast laser induced electron emission from a metal tip *Phys. Plasmas* **20** 056705
[24] Bormann R, Gulde M, Weismann A, Yalunin S and Ropers C 2010 Tip-enhanced strong-field photoemission *Phys. Rev. Lett.* **105** 147601
[25] Krüger M, Schenk M and Hommelhoff P 2011 Attosecond control of electrons emitted from a nanoscale metal tip *Nature* **475** 78–81
[26] Herink G, Solli D R, Gulde M and Ropers C 2012 Field-driven photoemission from nanostructures quenches the quiver motion *Nature* **483** 190–3
[27] Park D J, Piglosiewicz B, Schmidt S, Kollmann H, Mascheck M and Lienau C 2012 Strong field acceleration and steering of ultrafast electron pulses from a sharp metallic nanotip *Phys. Rev. Lett.* **109** 244803
[28] Mueller B Y and Rethfeld B 2013 Relaxation dynamics in laser-excited metals under nonequilibrium conditions *Phys. Rev.* B **87** 035139
[29] Pant M and Ang L K 2013 Time-dependent quantum tunneling and nonequilibrium heating model for the generalized Einstein photoelectric effect *Phys. Rev.* B **88** 195434
[30] Wendelen W, Autrique D and Bogaerts A 2010 Space charge limited electron emission from a Cu surface under ultrashort pulsed laser irradiation *Appl. Phys. Lett.* **96** 051121
[31] Wendelen W, Mueller B Y, Autrique D, Rethfeld B and Bogaerts A 2012 Space charge corrected electron emission from an aluminum surface under non-equilibrium conditions *J. Appl. Phys.* **111** 113110
[32] Lau Y Y 2001 Simple theory for the two-dimensional Child–Langmuir law *Phys. Rev. Lett.* **87** 278301
[33] Nieter C and Cary J R 2004 VORPAL: a versatile plasma simulation code *J. Comput. Phys.* **196** 448–73
[34] Mahalingam S, Nieter C, Loverich J, Smithe D and Stoltz P 2009 Space charge limited currents calculations in coaxial cylindrical diodes using particle-in-cell simulations *Open Plasma Phys. J.* **2** 7
[35] Chen S H, Tai L C, Liu Y L, Ang L K and Koh W S 2011 Two-dimensional electromagnetic Child–Langmuir law of a short-pulse electron flow *Phys. Plasmas* **18** 023105
[36] Zhu Y B, Zhang P, Valfells Á, Ang L K and Lau Y Y 2013 Novel scaling laws for the Langmuir–Blodgett solutions in cylindrical and spherical diodes *Phys. Rev. Lett.* **110** 265007
[37] Sun S and Ang L K 2012 Onset of space charge limited current for field emission from a single sharp tip *Phys. Plasmas* **19** 033107